Mar Geophys Res (2017) 38:47–60
DOI 10.1007/s11001-016-9292-1

ORIGINAL RESEARCH PAPER

Mantle source heterogeneity and magmatic evolution at Carlsberg Ridge (3.7°N): constrains from elemental and isotopic (Sr, Nd, Pb) data

Ling Chen[1] · Limei Tang[1,2] · Xing Yu[1] · Yanhui Dong[1]

Received: 27 May 2016 / Accepted: 7 November 2016 / Published online: 24 December 2016

Abstract We present new major element, ICP-MS trace element, and Sr–Nd–Pb isotope data of basalts from four locations along the Carlsberg Ridge (CR), northern Indian Ocean. The basalts are low-K tholeiites with 7.52–9.51 wt% MgO, 49.40–50.60 wt% SiO_2, 0.09–0.27 wt% K_2O, 2.55–2.90 wt% Na_2O, and 0.60–0.68 $Mg^{\#}$. Trace element contents of the basalts show characteristics similar to those of average normal MORB, such as LREE depleted patterns with $(La/Sm)_N$ ratio of 0.55–0.69; however, some samples are enriched in large-ion lithophile elements such as K and Rb, suggesting probable modification of the mantle source. Poor correlations between the compatible elements [e.g. Ni, Cr, and Sr (related to olivine, clinopyroxene and plagioclase, respectively)] and the incompatible elements (e.g. Zr and Y), and positive correlations in the Zr versus Zr/Y and Nb versus Nb/Y plots suggest a magmatic evolution controlled mainly by mantle melting rather than fractional crystallization. Our results extend the CR basalt range to higher radiogenic Pb isotopes and lower $^{143}Nd/^{144}Nd$. These basalts and basalts from the northern Indian Ocean Ridge show lower $^{143}Nd/^{144}Nd$ and higher $^{87}Sr/^{86}Sr$ values than those of the depleted mantle (DM), defining a trend towards pelagic sediment composition. The Pb isotopic ratios of basalts from CR 3–4°N lie along the compositional mixing lines between the DM and the upper continental crust. However, the low radiogenic Pb of basalts from CR 9–10°N lie on the mixing line between the DM and lower continental crust. Since the Pb isotopic ratio of MORB would decrease if the source mantle was contaminated by continental lithospheric mantle, we suggest that CR contains continental lithospheric material, resulting in heterogeneous mantle beneath different ridge segments. The continental lithospheric material was introduced into the asthenosphere before or during the breakup of the Gondwana. These results support the long-term preservation of continental material in the oceanic mantle which would significantly influence the isotopic anomaly of the Indian Ocean MORB.

Keywords Sr–Nd–Pb isotopes · Mantle melting · Mantle heterogeneity · Mantle contamination · Carlsberg Ridge

Introduction

The Indian Ocean Ridge system (IORS) is an upside-down "Y"-shaped ridge system with three main oceanic ridges: the northern Indian Ocean Ridge, the Southwest Indian Ridge (SWIR), and the Southeast Indian Ridge (SEIR) (Fig. 1). These three ridges intersect at the Rodriguez Triple Junction (RTJ; 25°30′S, 70°E; Humler and Whitechurch 1988; Munschy and Schlich 1989) (Fig. 1). The northern Indian Ocean Ridge can be further subdivided into four ridge segments: from north to south they are the Gulf of Aden spreading center, the Carlsberg Ridge (CR), Northern Central Indian Ridge (NCIR), and Southern Central Indian Ridge (SCIR) (Patriat et al. 1997; Ray et al. 2013) (Fig. 1). CR has the lowest half spreading rate (~11–16 mm/year) in the northern Indian Ocean Ridge system (Chaubey et al. 1993; Ramana et al. 1993; Raju

✉ Limei Tang
tanglm@sio.org.cn

[1] SOA Key Laboratory of Submarine Geoscience, Second Institute of Oceanography, State Oceanic Administration, Hangzhou 310012, People's Republic of China

[2] Present Address: Second Institute of Oceanography, State Oceanic Administration, 36 Northern Baochu Road, Hangzhou 310012, People's Republic of China

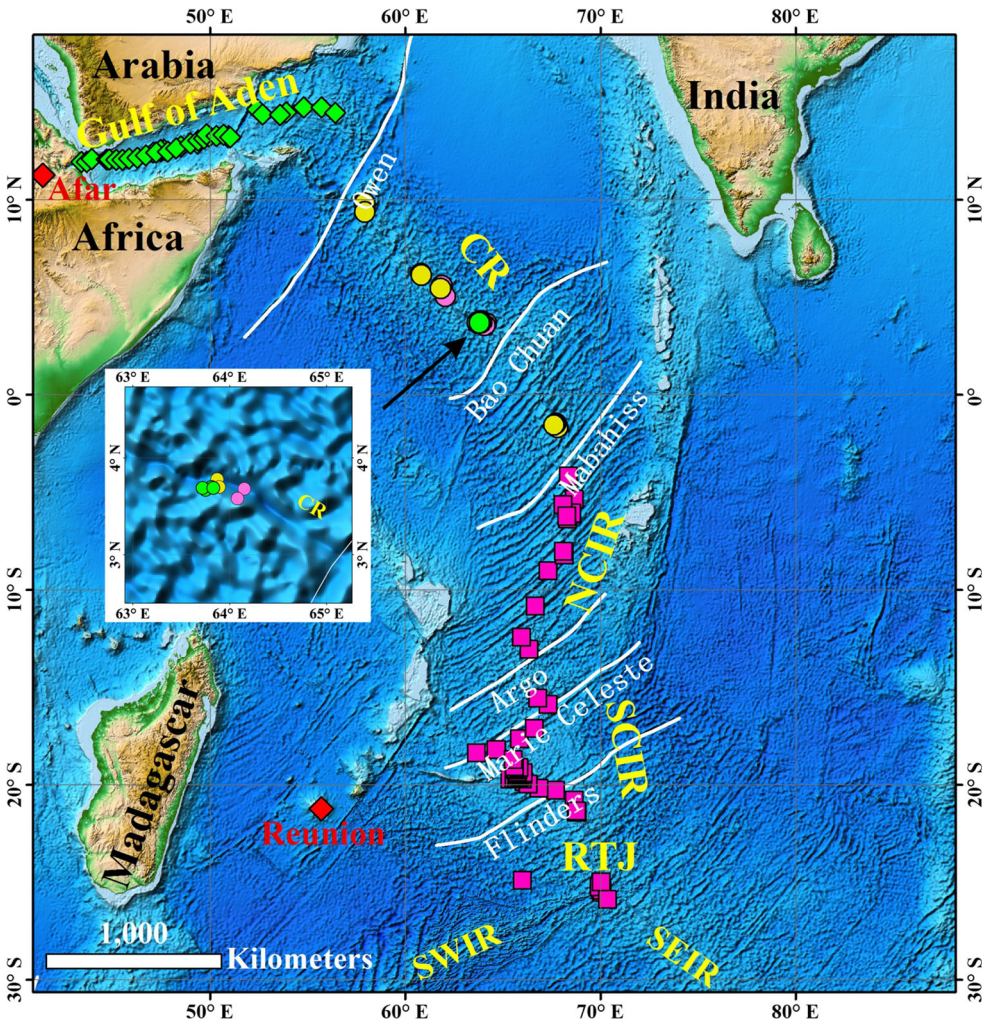

Fig. 1 Bathymetric map showing the ridge system of the northern Indian Ocean. Sample locations of this study are shown as *green circles* and the *inset* shows detailed information of the sampling area. Other stations of published basalts (*green diamonds* for the Gulf of Aden, *circles* for CR, and *squares* for CIR-RTJ) are also shown. *Yellow circles* are used to discriminate stations with basalts having isotopic data from other CR stations (*pink circles*). Fracture zones (*white lines*) and hot spots (*red diamonds*) are also shown. *CR* Carlsberg Ridge, *CIR* Central Indian Ridge, *RTJ* Rodrigues Triple Junction, *SWIR* Southwest Indian Ridge, *SEIR* Southeast Indian Ridge

et al. 2008); there are relatively few studies on CR (e.g. Mahoney et al. 1992; Ray et al. 2013), even compared to the other Indian Ocean spreading centers.

Previous studies confirmed that mid-ocean ridge basalts (MORB) in the Indian Ocean differ from Atlantic and Pacific MORB in terms of Sr, Nd, and Pb isotopic composition (e.g. Dupré and Allègre 1983; Hart 1984). MORB in the Indian Ocean display a greater degree of isotopic heterogeneity per given length of ridge than in the Atlantic and far more than in the Pacific (Mahoney et al. 1992; Meyzen et al. 2007), for example, a well-defined upper mantle domain with higher $^{87}Sr/^{86}Sr$ and lower $^{143}Nd/^{144}Nd$ were identified in the Indian Ocean mantle. This domain extends under the CR-CIR (Rehkämper and Hofmann 1997; Nauret et al. 2006), and its northern arm extends into the Gulf of Aden (Rooney et al. 2012). Several different hypotheses have been proposed to explain the distinct isotopic characteristics of the upper mantle domain. Isotopic evidences of MORB from the Gulf of Aden indicate that sub-ridge mantle was contaminated by the Afar plume (Rooney et al. 2012). Studies of the CR-CIR suggest that the influence of the Reunion plume on the southern CIR accounts for the highly enriched compositions that exist between latitude 18°S and 20°S (Dyment et al. 2001; Escrig et al. 2004; Murton et al. 2005; Nauret et al. 2006; Füri et al. 2011). Additionally, Ray et al. (2013) proposed that the geochemistry of the CR-CIR MORB was governed by the oceanic upper mantle contaminated by ancient continental crust.

At present, few papers have been published on CR MORB (e.g. Subbarao et al. 1979; Mahoney et al. 1992; Ray et al. 2013), especially on their Sr–Nd–Pb isotopic composition; moreover, there is no study that compares MORB from different segments of the internal CR. CR MORB are regarded as compositionally distinct from IORS MORB having typical N-MORB characteristics (Subbarao et al. 1979). However, previously acquired detailed geochemical data of MORB from several locations on the CR are still inadequate to understand their petrogenetic evolutionary process (e.g. Dupré and Allègre 1983; Mahoney et al. 1989, 1992; Ray et al. 2013). Since the CR mantle is an important part of the distinct Indian Ocean mantle

domain, more geochemical data of MORB are required to investigate the mantle source and melt evolution beneath the poorly studied CR. Comparison of MORB from different segments of the CR will give a new and detailed sight to the diversity of mantle composition and magmatic process within the CR. Additionally, a general comparison of MORB from different parts of the northern Indian Ocean Ridge is helpful to investigate the different influencing factors during the genesis of the Indian Ocean MORB. So in this study, we present new geochemical data of MORB from four different locations on CR (Fig. 1), including Sr–Nd–Pb isotope data, and perform a geochemical comparison between MORB from different segments of the CR and the northern Indian Ocean Ridge to investigate their petrogenetic processes and mantle source composition.

Sampling and petrography

The Carlsberg Ridge (ridge length ~2000 km) is characterized by rugged topography, steep inner valley walls and a wide rift valley floor similar to the slow-spreading ridge segment of the northern mid-Atlantic Ridge (MAR). CR has a NW–SE orientation that becomes more N–S at its southern end (Fig. 1), with non-transform discontinuities and along-axis bathymetric deeps (Ramana et al. 1993; Ray et al. 2013). The study area is located in the middle portion of the CR; the samples were collected from four sites (3.70°N, 63.81°E; 3.67°N, 63.75°E; 3.69°N, 63.72°E; and 3.69°N, 63.83°E) by Television Grab during the DY125-26 cruise in 2012 (Fig. 1). These samples are all pillow basalts and have a black surface with patches of brown iron and manganese (Fig. 2a, c). Except for one sample (CR03-2) with ~1 cm thick glassy rim (Fig. 2a), other samples are fine-grained basalts largely lacking fresh glassy rims due to alteration (e.g. Fig. 2c). Thin sections of the fresh samples show that some samples consist of aphanitic glass with a few tiny plagioclases and olivine phenocrysts (Fig. 2b), while others have typical basaltic structure with interstitial pyroxene in triangular lattices composed of acicular plagioclase (e.g. Fig. 2d).

Analytical techniques

The fresh samples were selected and crushed to powder of 200 mesh in agate mortars at the Second Institute of Oceanography, State Oceanic Administration, Hangzhou, China. Glass and whole-rock major and trace element analysis was performed at ALS Minerals in Guangzhou, China. The major elements were analyzed by X-ray fluorescence (XRF); the analytical precision was better than ±2–5%. The trace elements were determined by inductively coupled plasma mass spectrometry (ICP-MS) after complete dissolution. The analytical precision for most of the trace elements was better than ±5%. Two rock standards (kinzingite SARM-45 and kiorite Gneiss SY-4) and two randomly selected repeat samples were chosen to monitor the data quality and reproducibility.

Sr–Nd–Pb isotope analysis was carried out by multicollector ICP-MS (Neptune MC-ICP-MS, Thermo Scientific) using internal standardization and external calibration with bracketing isotope SRMs (ALS Scandinavia, Luleå, Sweden). The samples were digested by HNO_3 + HF in closed Teflon vials at 160 °C for 48 h; the digests were then dried and the excess F component was removed by addition of concentrated HNO_3 and evaporation until dry (the procedure was repeated three times). The solid residue was re-dissolved with HCl by heating in closed vials at 160 °C for 1 h, and then evaporated until dry. All the samples were digested in duplicates, one for further process by Pb–Sr column separation, and one for further process by Nd column separation. For samples with high Sr and Nd concentrations where no Pb IRMs was required, alkali fusion was used for sample preparation. For Sr and Pb column separation, the residues from the above digestion-drying process were taken up in 70% HNO_3 followed by Sr and Pb separation using Sr-specific Eichrom ion-exchange columns where the Sr was eluted in 0.01 M HNO_3 and the Pb in a EDTA solution. After purification, each element fraction was dried and re-dissolved in 5% HNO_3, ready for isotope analyses. In the process, ICP-SFMS was used for testing concentration and MC-ICP-MS was used to test isotopes. Where possible, the Sr and Pb concentrations were adjusted to 0.2–0.1 ppm, respectively, by dilution. For Nd column separation, the residues from the above digestion–drying process were taken up in 1 M HCl, then the rare earth elements (REEs) as a group were separated from the sample matrix solution by AG50-X8 cation exchange resin, evaporated until dry, re-dissolved in 0.4 M HNO_3, and the Nd separated from the Sm by using a Ln Resin (Eichrom) chromatography column. After purification, the Nd fraction solution was analyzed by ICP-SFMS and the analyte concentration was adjusted to a Nd concentration of 0.1 ppm. The Sr and Nd isotope ratios were normalized to $^{86}Sr/^{88}Sr = 0.1194$ and $^{146}Nd/^{144}Nd = 0.7219$, respectively. During the analyses, the NBS987 Sr isotope standard yielded a $^{87}Sr/^{88}Sr$ value of 0.710266 ± 0.000006 (2σ, n = 2). The measured Nd isotope standard Thermo Nd yielded a $^{143}Nd/^{144}Nd$ ratio of 0.512420 ± 0.000009 (2σ, n = 2). The measured $^{206}Pb/^{204}Pb$, $^{207}Pb/^{204}Pb$, and $^{208}Pb/^{204}Pb$ ratios of standard NBS981 were 16.9374 ± 0.0085, 15.4916 ± 0.0076, and 36.7219 ± 0.0182 (2σ, n = 2), respectively. The standard deviations (SD) are reported from repeated analysis of each sample.

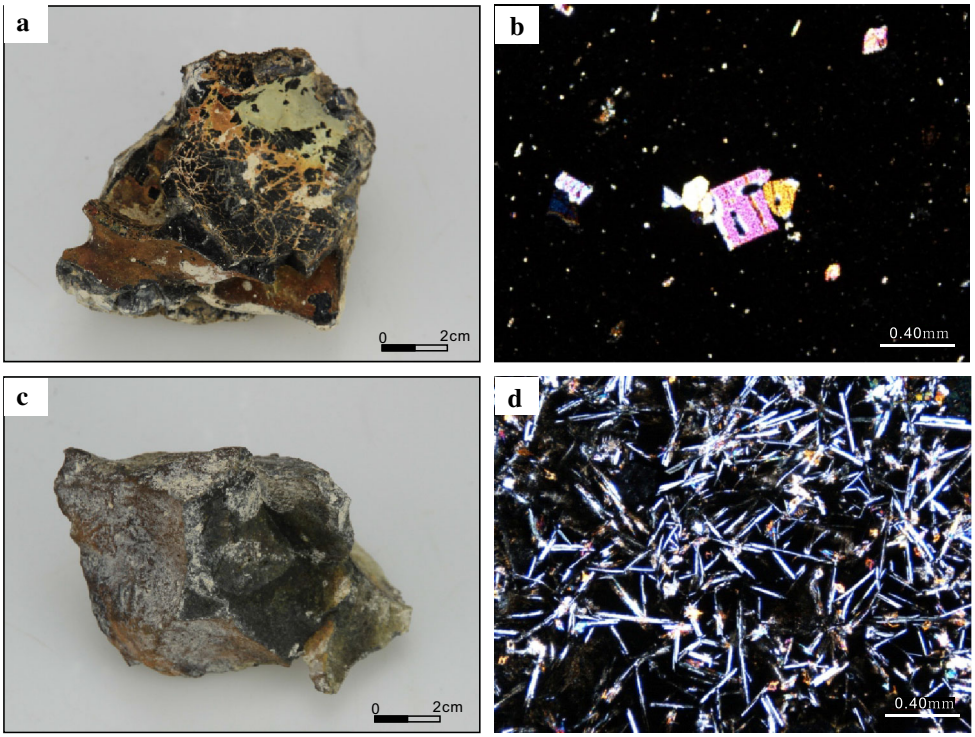

Fig. 2 Hand specimens (**a**, **c**) and photomicrographs (**b**, **d**) of glassy MORB from the CR; **b** tiny plagioclase and olivine phenocrysts in glasses; **d** quenched plagioclase laths in glassy MORB

Geochemistry

Major elements

The major and trace element data of the CR basalts are shown in Table 1. The samples analyzed in this study belong to the low-K series with MgO contents of 7.52–9.51 wt%, SiO_2 contents of 49.40–50.60 wt%, K_2O contents of 0.09–0.27 wt%, and Na_2O contents of 2.55–2.90 wt%. The samples were relatively fresh with low LOI and a narrow range of $Mg^{\#}$ (0.60–0.68) (Table 1), and belong to the mid-Ti basalts (1.22–1.64 wt%) (Natland 1991). The Na_2O, K_2O, and TiO_2 content of the samples decreased with increasing MgO content, while the content of SiO_2, Al_2O_3, and CaO are relatively uniform in all samples (Fig. 3). Different segments of CR from north to south (10°N to 2°S) showed different composition characteristics, and the major elements varied widely with the lowest alkali in basalts from 9 to 10°N segment (Fig. 3). However, the MgO content of all the samples from CR is relatively high (about 7–10 wt%), indicating a lower degree of magma fractionation. The major element compositions of the samples from this study are consistent with those previously reported from the 3–4°N region of CR (Fig. 3).

Trace elements

The chondrite normalized REE diagram (Fig. 4a) shows that all the CR samples have light REE (LREE)-depleted patterns typical of N-MORB, but the samples from the 9 to 10°N segment are most depleted in LREE, while the CR samples of this study and samples from the 3 to 4°N segment are somewhat less depleted in LREE [$(La/Sm)_N = 0.55–0.68$] and have flat heavy REE (HREE) patterns [$(Ce/Yb)_N = 0.84–1.08$)].

The N-MORB-normalized incompatible element diagram (Fig. 4b) shows that CR basalts from different segments have different patterns. The 9–10°N segment samples and some 1–2°S segment samples are more depleted in some large-ion lithophile elements (LILE) than N-MORB, but the composition of the samples from this study and from the 3 to 4°N segment are similar to those of N-MORB, except for some samples that are enriched in LILE (such as Rb and K) (Fig. 4b); however, their $(La/Sm)_N$ ratios are far less than 0.15, which suggests that they cannot belong to E-MORB [$(La/Sm)_N > 0.15$ Gale et al. 2013].

Sr–Nd–Pb isotope

The Sr–Nd–Pb isotope data is shown in Table 2. The isotopic compositions of MORB from this study have the

Table 1 Representative major and trace element compositions of basalts from the CR

Sample	CR01	CR02-1	CR02-2	CR03-1	CR03-2	CR04-1	CR04-2
Major element (wt%)							
SiO_2	50.60	49.90	50.10	49.50	49.40	50.30	50.00
Al_2O_3	15.40	14.85	14.80	15.50	15.40	14.80	15.15
$Fe_2O_3^T$	9.60	10.70	11.15	9.62	9.75	10.90	9.67
MnO	0.16	0.18	0.19	0.18	0.23	0.18	0.17
MgO	7.92	7.52	7.65	9.40	9.51	8.35	7.84
CaO	11.25	10.70	10.75	11.25	11.25	10.85	10.80
Na_2O	2.76	2.88	2.84	2.55	2.59	2.86	2.90
K_2O	0.18	0.27	0.27	0.12	0.12	0.13	0.09
TiO_2	1.43	1.63	1.64	1.22	1.23	1.60	1.49
P_2O_5	0.13	0.15	0.16	0.11	0.11	0.15	0.13
LOI	0.21	−0.01	0.08	−0.36	−0.42	−0.61	0.61
K/Ti	0.13	0.17	0.16	0.10	0.10	0.08	0.06
$Mg^{\#}$	0.64	0.61	0.60	0.68	0.68	0.63	0.64
Trace element (ppm)							
Sc	33.7	34.4	35.7	33.6	33.4	38.6	41.4
V	261	287	295	250	245	272	274
Cr	298	208	219	325	321	235	220
Co	43.9	126.5	45.5	58.3	54.7	56.1	99.9
Ni	143.0	118.0	126.5	227	240	153.5	127.5
Cu	69.2	66.2	65.2	75.0	86.2	68.2	185.0
Zn	95	93	94	80	85	81	454
Ga	16.40	17.20	17.90	16.10	15.95	16.55	16.40
Ge	0.11	0.15	0.14	0.14	0.13	0.07	0.08
Rb	1.1	3.6	4.1	1.0	1.4	0.9	0.6
Sr	131	121	129	112.5	120	123.5	115.5
Y	31.1	34.9	35.9	26.4	27	33.9	32.1
Zr	101.5	120	127.5	87	89.1	110.5	98.3
Nb	2.5	3.2	3.2	2.3	2.4	2.6	2
Ba	8.9	12.5	15.1	12.3	17.9	10.6	6.5
Hf	2.7	3.2	3.2	2.2	2.3	3.1	2.8
Ta	0.2	0.4	0.2	0.2	0.2	0.4	0.2
Th	0.17	0.28	0.32	0.27	0.29	0.24	0.18
U	0.20	0.11	0.14	0.09	0.09	0.08	0.08
La	3.5	4.3	4.6	3	3.2	3.8	3.3
Ce	10.2	12.65	14.65	10.35	11	11.6	10.15
Pr	1.87	2.16	2.31	1.58	1.62	2.13	1.82
Nd	10.7	12.2	12.4	8.7	9	11.6	10.4
Sm	3.59	4.26	4.38	3.1	2.99	4.09	3.86
Eu	1.3	1.41	1.5	1.03	1.14	1.4	1.39
Gd	4.83	5.54	5.75	4.03	4.18	5.42	4.97
Tb	0.89	1.01	1.04	0.74	0.78	0.99	0.9
Dy	5.54	6.32	6.35	4.9	4.91	6.15	5.9
Ho	1.25	1.42	1.42	1.07	1.08	1.36	1.28
Er	3.48	3.89	3.98	2.93	3.03	3.75	3.65
Tm	0.51	0.58	0.6	0.45	0.46	0.6	0.55
Yb	3.36	3.62	3.98	3.01	2.83	3.75	3.37
Lu	0.53	0.55	0.59	0.44	0.46	0.58	0.54
$(La/Sm)_N$	0.63	0.65	0.68	0.62	0.69	0.60	0.55

$Mg^{\#} = Mg/Mg + Fe^{2+}$, $(La/Sm)_N$: chondrite-normalized (Sun and McDonough 1989) value

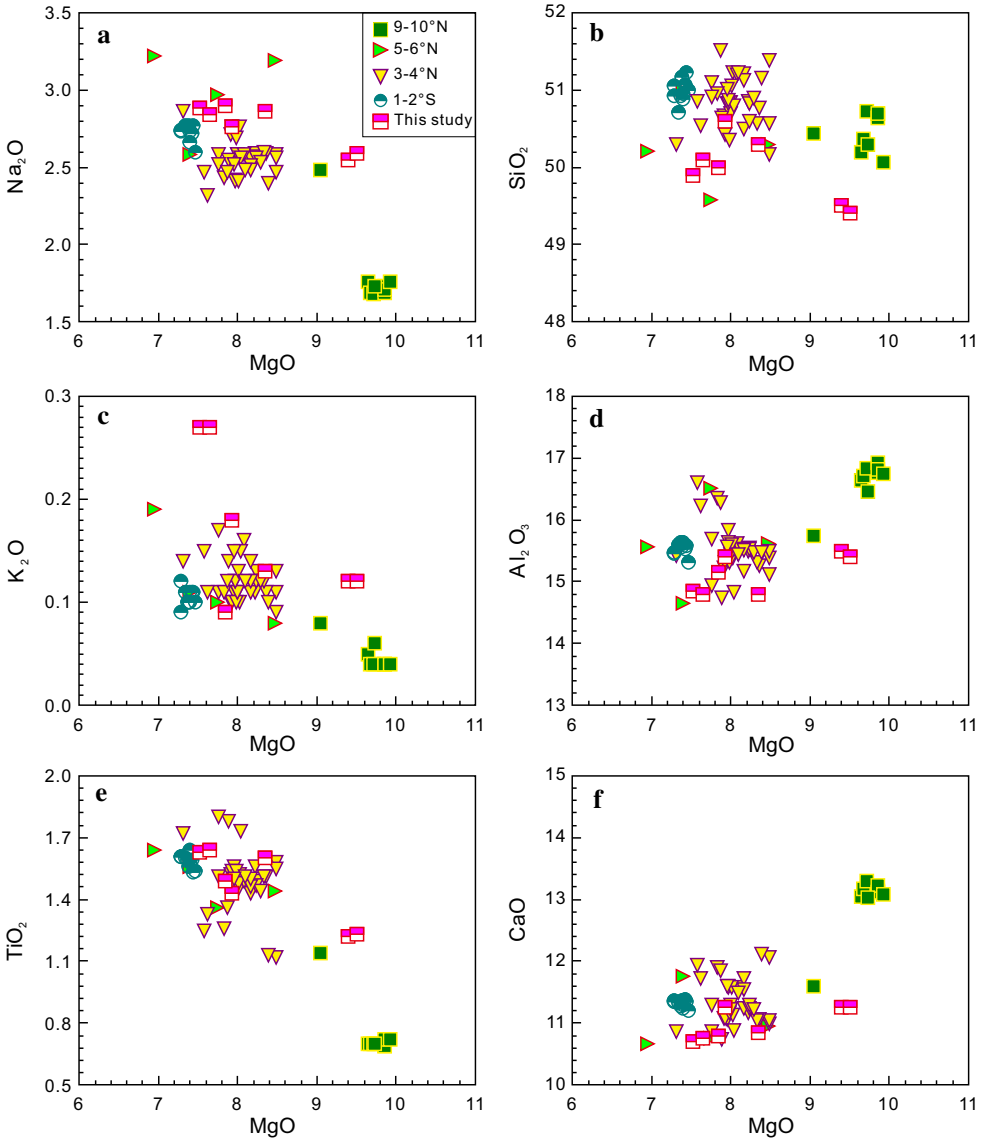

Fig. 3 Major elements versus MgO (all in wt%) diagrams. The CR basalts data for comparison with our samples are from Hekinian (1968), Cann (1969), Cohen and O'Nions (1982), Banerjee and Iyer (1991), Melson et al. (2002), Jenner and O'Neill (2012), and Ray et al. (2013)

highest radiogenic Pb and lowest Nd isotopic ratios within the CR basalts, which extends the published composition range of CR basalts (Fig. 5). Comparison with the Pacific and Atlantic MORB shows that the isotopic compositions of the northern Indian Ocean Ridge basalts have little overlap with those of the Pacific MORB, with relatively higher $^{87}Sr/^{86}Sr$ and lower $^{143}Nd/^{144}Nd$ (Fig. 5b). Additionally, the $^{87}Sr/^{86}Sr$ of the CR basalts is closer to that of NCIR and RTJ basalts with a range of 0.70257–0.70298, while the $^{87}Sr/^{86}Sr$ of the SCIR and Gulf of Aden MORB has a larger variation, from 0.70268 to 0.70411 (Fig. 5b). In the $^{206}Pb/^{204}Pb$ versus $^{207}Pb/^{204}Pb$ and $^{206}Pb/^{204}Pb$ versus $^{208}Pb/^{204}Pb$ diagrams (Fig. 5c, d), most of the northern Indian Ocean Ridge basalts are distributed on the mixing lines between the depleted mantle (DM) and upper continental crust (UCC) or enriched mantle II (EM2) whereas some basalts are near the mixing line defined by the DM and lower continental crust (LCC). Different segments of CR have different isotopic ratios (Fig. 5): the 9–10°N segment basalts are characterized by the lowest Pb isotopic ratios compared to the northern Indian Ocean Ridge basalts; basalts from this study (near 3.7°N) extend the CR MORB to higher radiogenic Pb and are distributed along the mixing line between the DM and UCC data; other basalts from the 3 to 6°N and 1 to 2°S segments are closer to the DM compositions despite the slightly higher Pb isotopic ratios. These observations suggest that the isotopic variation of CR MORB is wide and extends to the least radiogenic Pb end member within the northern Indian Ocean Ridge basalts.

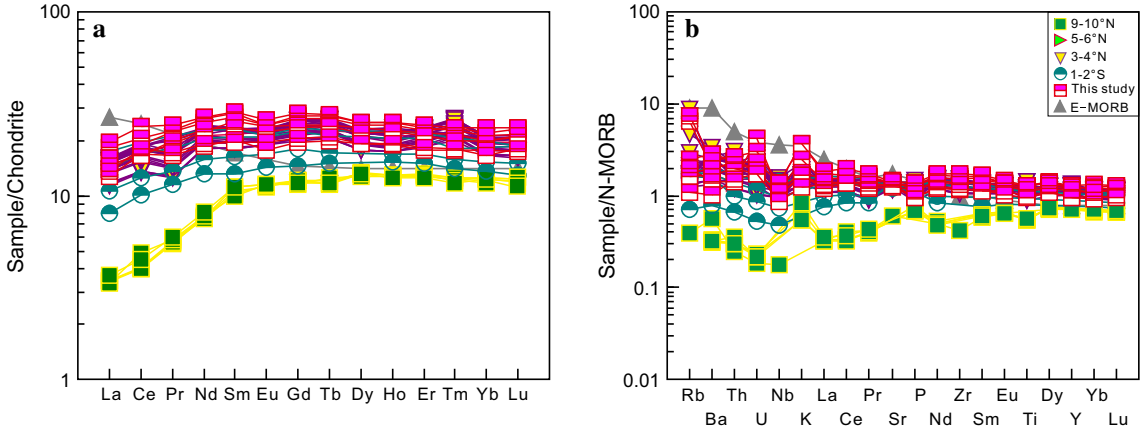

Fig. 4 Chondrite-normalized rare earth element (REE) diagram (**a**) and N-MORB-normalized spider diagram (**b**) of CR basalts. The compositions of chondrite, E-MORB, and N-MORB are from Sun and McDonough (1989). Other data are from Jenner and O'Neill (2012), Gale et al. (2013), and Ray et al. (2013)

Table 2 Sr–Nd–Pb isotopic compositions of CR basalts

Sample	Location	$^{87}Sr/^{86}Sr$	$^{143}Nd/^{144}Nd$	$^{206}Pb/^{204}Pb$	$^{207}Pb/^{204}Pb$	$^{208}Pb/^{204}Pb$	Segment	References
CR01	3.70°N, 63.81°E	0.702808 ± 7	0.513084 ± 6	18.223	15.535	38.066	3–4°N	This study
CR02-2	3.67°N, 63.75°E	0.702927 ± 13	0.513076 ± 13	18.457	15.588	38.475	3–4°N	This study
CR03-1	3.69°N, 63.72°E	0.702942 ± 7	0.513038 ± 5	18.463	15.585	38.476	3–4°N	This study
13Dr	6.15°N, 60.85°E	0.702574 ± 6	0.513077 ± 12	18.157	15.450	37.822	5–6°N	Rehkämper and Hofmann (1997)
23Dr	1.55°S, 67.61°E	0.702772 ± 6	0.513067 ± 8	18.149	15.472	38.001	1–2°S	Rehkämper and Hofmann (1997)
24Dr	1.51°S, 67.66°E	0.702865 ± 8	0.513063 ± 12	18.041	15.451	37.838	1–2°S	Rehkämper and Hofmann (1997)
25Dr	1.48°S, 67.70°E	0.702841 ± 8	0.513055 ± 11	18.000	15.443	37.781	1–2°S	Rehkämper and Hofmann (1997)
078-I5.27 N	5.45°N, 61.83°E	0.70266	0.51312	18.240	15.440	37.810	5–6°N	Cohen and O'Nions (1982)
VG5262	3.78°N, 63.87°E	0.70283	0.51307	17.978	15.451	37.760	3–4°N	Ito et al. (1987)
VG5284	1.65°S, 67.77°E	0.70284	0.51311	17.997	15.460	37.816	1–2°S	Ito et al. (1987)
VG5269	3.70°N, 63.89°E	0.70274	0.5131	18.009	15.473	37.846	3–4°N	Ito et al. (1987)
VG5252	9.38°N, 57.95°E	0.70267	0.51318	17.335	15.370	37.084	9–10°N	Mahoney et al. (1992)
NOAA 3-10	9.83°N, 57.95°E	0.70262		17.353	15.425	37.19	9–10°N	Dupré and Allègre (1983)

Discussion

The isotopic composition of the Indian Ocean MORB is different from that of the Pacific MORB and Atlantic MORB which have, on average, relatively higher $^{87}Sr/^{86}Sr$ and lower $^{143}Nd/^{144}Nd$ and $^{206}Pb/^{204}Pb$ ratios (Dupré and Allègre 1983; Hart 1984). Diversity in mantle source composition was thought to be the major reason for these differences (Ito et al.1987; Mahoney et al. 1992; Hofmann 2003). MORB samples from different ridges in the northern Indian Ocean show obvious variation in isotopic composition (Fig. 5), which is consistent with the observation that the mantle domain of the Indian Ocean MORB is more compositionally heterogeneous than that of the Pacific MORB (Mahoney et al. 1989; Rehkämper and Hofmann 1997; Escrig et al. 2004; Hofmann 2003; Sang et al. 2014). In the CR basalts, significant compositional variations can also be observed among the different ridge segments (Figs. 3, 5). Since mantle source is not the only factor that influences the basalt composition, in the

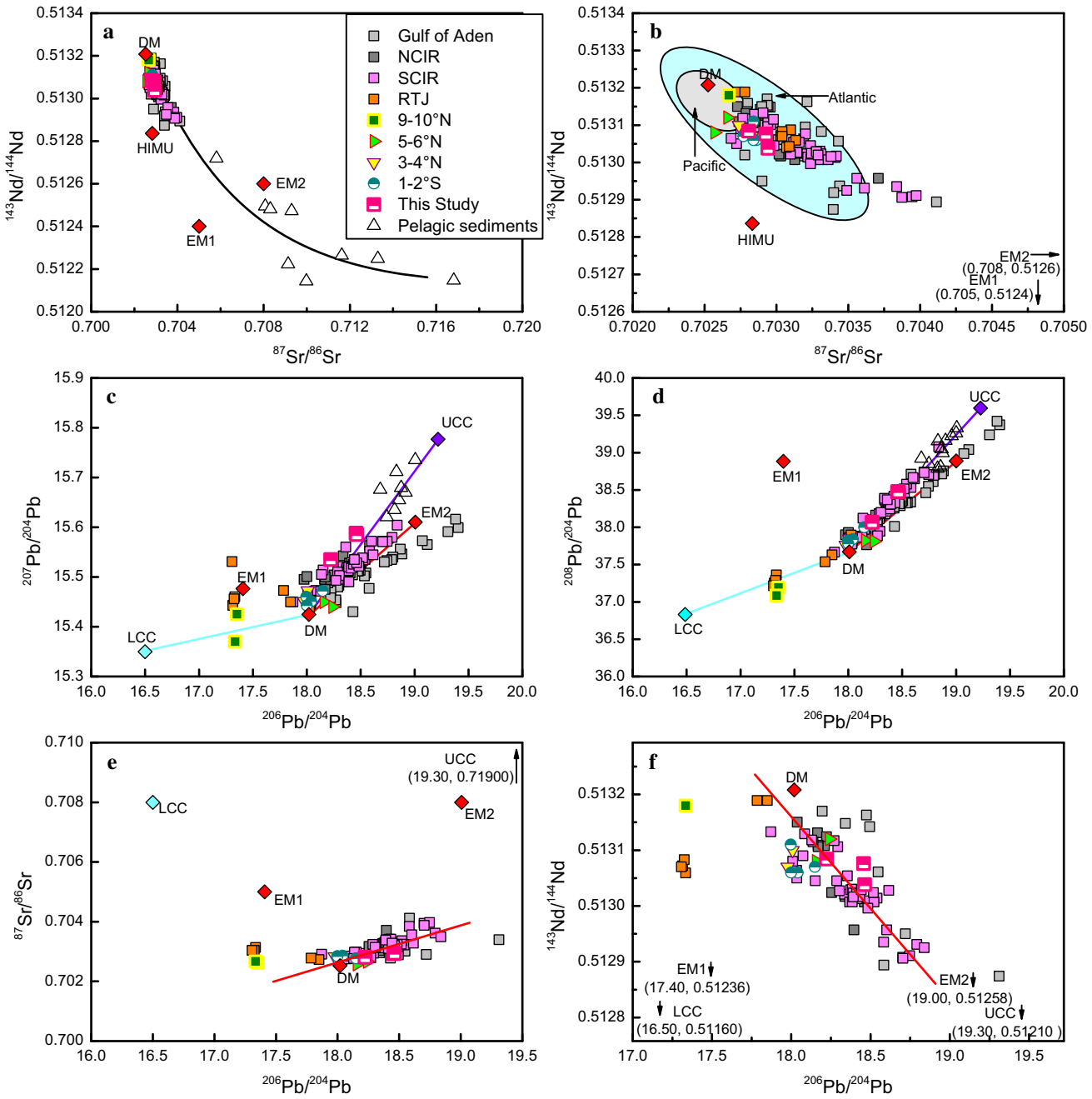

Fig. 5 Sr–Nd–Pb isotopes diagrams for basalts from the northern Indian Ocean Ridge. *Data sources* Pelagic sediments: Othman et al. (1989); DM: Hart (1984); HIMU, EM1 and EM2: Armienti and Gasperini (2007); LCC: Escrig et al. (2004); UCC: Hemming and McLennan (2001); CR: as shown in Table 2; the Gulf of Aden: Schilling et al. (1992); NCIR: Ito et al. (1987), Mahoney et al. (1989), Escrig et al. (2004), and Ray et al. (2014); SCIR: Mahoney et al. (1989), Rehkämper and Hofmann (1997), Escrig et al. (2004), and Nauret et al. (2006); RTJ: Michard et al. (1986), Price et al. (1986), and Ito et al. (1987). Additional data are from PetDB

following sections we examine the magmatic differentiation and partial melting of the CR basalts and the mantle source and discuss the cause of the compositional variations in CR basalts.

Fractional crystallization

The CR basalts in this study have small amounts of plagioclase phenocrysts and olivine phenocrysts (Fig. 2).

However, most of the CR basalts have MgO content higher than 7 wt% (Fig. 3), indicating that the fractional crystallization of the parent magma is not extensive. The negative anomaly of Eu is also slight in CR basalts (Fig. 4), which excludes the possibility of significant crystallization of plagioclase. The fractional crystallization of clinopyroxene phenocrysts can decrease the content of HREE in basaltic magma (White 1991); however, the flat HREE pattern in our data suggests no major fractionation of clinopyroxene from the CR parent magmas (Fig. 4). In addition to the REE results, Fig. 6 shows that the Ni and Cr concentrations in the CR basalt specimens tend to decrease with increasing Y and Zr, which suggests crystallization of olivine and clinopyroxene of the parent magmas (Winter 2001). In contrast, Sr shows no significant change with Y and Zr, indicating weak fractional crystallization of the plagioclase (Fig. 6). Our results are consistent with published CR basalt data although the compositional trend is not so obvious in the published data. Generally, the combination of the data of the major and trace elements suggests that the CR basalts experienced minor rather than large-scale magmatic differentiation, and probably experienced only a moderate amount of olivine crystallization. This is consistent with the spreading rate (half spreading rate of 11–16 mm/year) of CR (Chaubey et al. 1993) because no large, stable magma chambers are present beneath the slow-spreading ridge (Dunn and Forsyth 2007), leading to less magmatic fractionation; thus, the MORB are more likely to preserve the information of the source mantle composition and mantle melting.

Mantle melting

The geochemistry of MORB is dominated by the source mantle composition, mantle melting, and fractional crystallization. In the $Mg^{\#}$ versus $(La/Sm)_N$ plot (Fig. 7a), the majority of CR MORB have $(La/Sm)_N$ values of $\sim$0.5 to $\sim$0.7 except for the 9–10°N MORB ($\sim$0.3); these data do not show any variation with decreasing $Mg^{\#}$, suggesting a DM source for the CR MORB. To eliminate the influence of fractional crystallization, we use Na_8 (Na_2O content corrected for fractional crystallization to a common MgO content of 8 wt%; Klein and Langmuir 1987) to investigate the influence of mantle melting on the magmatic evolution of CR MORB. As a moderately incompatible element, Na concentration in the melt decreases as the degree of melting increases (Klein and Langmuir 1987; Elthon 1992). Figure 7b shows a positive correlation between Na_8 and CaO/Al_2O_3, a further indicator of the degree of mantle melting (e.g. Condie 2003; Standish et al. 2008), suggesting that mantle melting plays a major role in controlling the major elements of the CR MORB (Fig. 7b). In the Zr versus Zr/Y (Fig. 7c) and Nb versus Nb/Y plots (Fig. 7d), the CR MORB samples show a strong positive correlation between the highly incompatible elements (Zr and Nb) and the highly incompatible/less incompatible element ratios (Zr/Y and Nb/Y), suggesting that Zr and Nb have more variability during mantle melting than Y, which is consistent with their higher incompatibility. This emphasizes the important role of mantle melting in controlling the trace element concentrations in CR MORB: fractional crystallization of MORB magma would cause similar variability of Zr and Y (Hofmann 2003); thus, Zr/Y will not show significant variation with rising Zr values.

In Na_8 versus CaO/Al_2O_3 plots (Fig. 7) the Na_8 of CR MORB show a large variation (1.4–4.2), indicating a great variability of the melting degree of the CR mantle. The mantle source composition greatly affects the initial melting depth; thus, the degree of melting depends on the fertility of the source mantle (Cannat et al. 2008; Meyzen et al. 2005). The initial compositional characteristics of MORB are derived from the mantle source even though subsequent compositional trends are controlled by mantle melting. However, mantle composition is thought to be heterogeneous beneath slow- and ultraslow-spreading ridges that contain enriched or/and DM component (e.g. Murton et al. 2005; Liu et al. 2008). The refractory mantle domains may be difficult to infer from MORB composition analysis because they would have been too depleted to melt during the most recent mantle melting. However, the addition of an enriched component to normal MORB mantle should be detected by MORB composition analysis, especially by isotope analysis (Meyzen et al. 2005; Nauret et al. 2006).

Implication for source contamination

The large variation in the major and trace elements of the CR MORB and the similarity of their characteristics to those of enriched MORB (E-MORB) in CR 3–4°N MORB (including the data obtained in this study) (Fig. 4b) suggest that the MORB mantle beneath CR may incorporate some enriched components. Previous studies indicated that the MORB mantle beneath the Indian Ocean was contaminated by various enriched components, such as hotspot material (Nauret et al. 2006), recycled subducted altered oceanic crust and/or sediment (Dupré and Allègre 1983; Cohen and O'Nions 1982; Rehkämper and Hofmann, 1997), ancient subcontinental lithospheric mantle (Mahoney et al. 1989; Escrig et al. 2004), and delaminated continental crust (Meyzen et al. 2005; Ray et al. 2013). The enriched components beneath CR can be further identified by the isotope data of the CR basalts.

Sr–Nd–Pb isotope data of MORB are very sensitive indicators for detecting mantle source composition and have been used to constrain the anomalous upper mantle

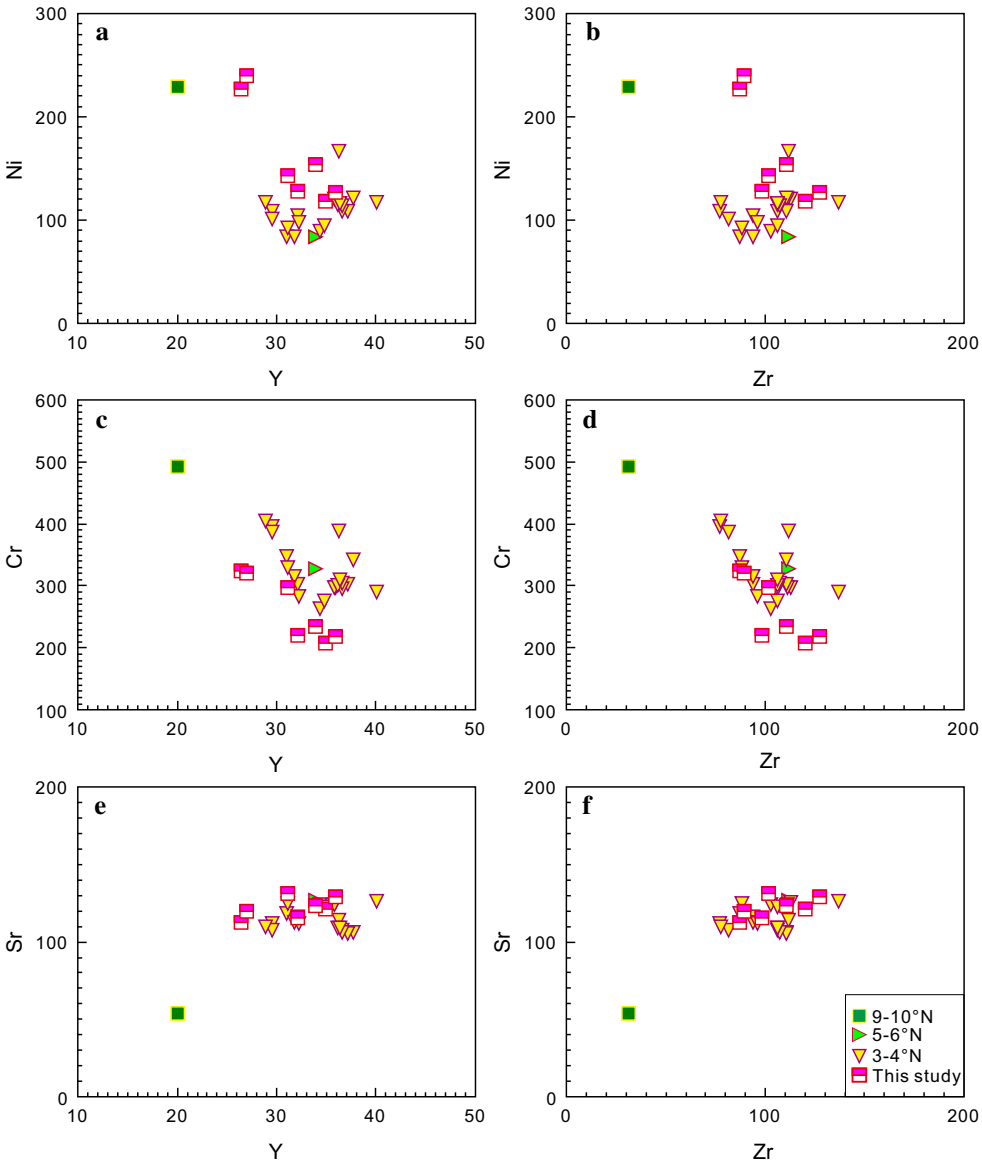

Fig. 6 Ni/Cr/Sr–Y and Ni/Cr/Sr–Zr diagrams for CR basalts. All elements are in ppm. *Data sources* are as in Fig. 4

beneath the Indian Ocean which shows higher $^{87}Sr/^{86}Sr$, $^{207}Pb/^{204}Pb$, $^{208}Pb/^{204}Pb$ and lower $^{143}Nd/^{144}Nd$ and $^{206}Pb/^{204}Pb$ compared to those ratios in the Atlantic and Pacific Oceans (Dupré and Allègre 1983; Hart 1984). In addition, the heterogeneity of the mantle is more obvious in both space and time in the Indian Ocean than in the other oceans (e.g. Meyzen et al. 2005; Mahoney et al. 1998; Janney et al. 2005), which may be related to the spreading rate and the presence of hotspots close to the ridge. The influence of hotspots on the ridge may be enhanced at slow- to ultraslow-spreading ridges (Mahoney et al. 1992) and the heterogeneity of the mantle may be reduced by the magma extraction processes associated with fast-spreading ridges (Cohen and O'Nions 1982). However, it is generally accepted that the variation of the MORB isotopic composition is mainly caused by the heterogeneity of the mantle source.

Basalts from different segments of the northern Indian Ocean Ridge have different isotopic compositions (Fig. 5). The Gulf of Aden and SCIR MORB have the largest variation in isotopic composition among the northern Indian Ocean Ridge basalts, having the highest $^{87}Sr/^{86}Sr$ and radiogenic Pb and the lowest $^{143}Nd/^{144}Nd$; Rooney et al. (2012) and Nauret et al. (2006) proposed that the mantle sources of these basalt groups may be influenced by material from the Afar and Reunion hotspots, respectively. In contrast, NCIR basalts show a narrower range of isotopic composition which may be due to the longer distance between the Reunion hotspot and NCIR compared to SCIR. The basalts from CR and RTJ which are relatively far from

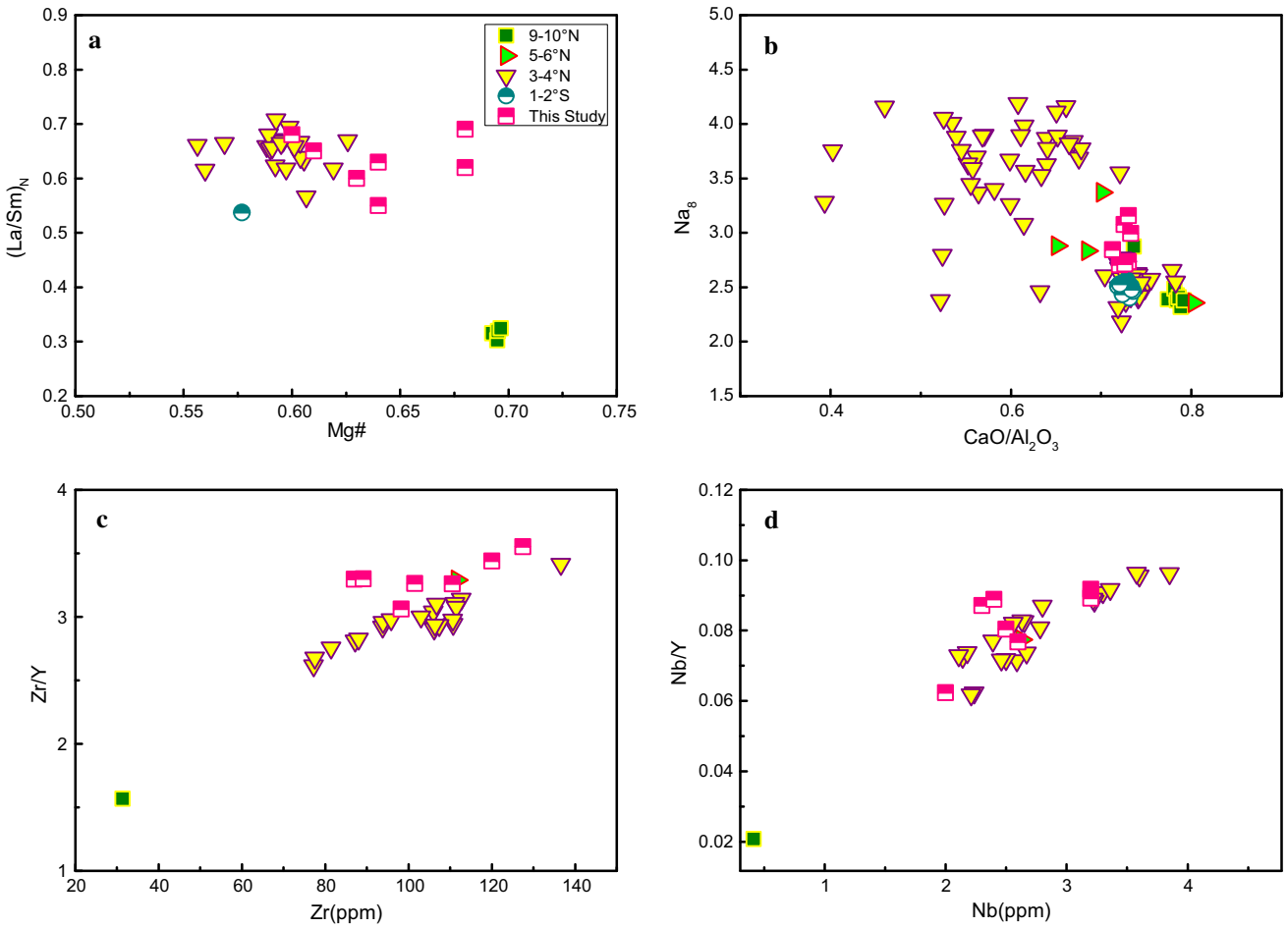

Fig. 7 $Mg^{\#}$–$(La/Sm)_N$ (**a**), CaO/Al_2O_3–Na_8 (**b**), Zr–Zr/Y (**c**) and Nb–Nb/Y (**d**) diagrams for CR basalts. *Data sources* are as in Fig. 4

the Afar and Reunion hotspots (Fig. 1) show small variations in Sr and Nd isotope ratios, closer to the composition of DM compared with basalts from other ridges (Fig. 5b). However, these basalts still have higher $^{87}Sr/^{86}Sr$ and lower $^{143}Nd/^{144}Nd$ than DM (Fig. 5b), which may indicate an enriched component in the mantle source. The enriched component which contaminates the CR mantle is less likely to be hotspot material because compared with the northern Indian Ocean Ridge basalts, the CR MORB has the lowest $^{87}Sr/^{86}Sr$ (<0.7030) which is far less than the SCIR basalts (Nauret et al. 2006) influenced by the Reunion hotspot ($^{87}Sr/^{86}Sr$ >0.7035; Escrig et al. 2004) (Fig. 5b). The ridge area that is most likely influenced by the hotspot is at the Marie Celeste Fracture Zone and on the adjacent ridge segment to the south; it is ~1100 km from the Reunion hotspot (Mahoney et al. 1989; Nauret et al. 2006), which is much less than the distance between the CR and the Reunion hotspot (>2000 km) (Fig. 1).

As shown in the Pb isotopic plots (Fig. 5c, d), most of the CIR MORB specimens lie on the mixing line between the DM and the UCC, which is consistent with contamination by the UCC component in the CIR mantle (Ray et al. 2013). The RTJ mantle may be contaminated by the LCC component as the basalts lie on the mixing line between the DM and the LCC in the $^{206}Pb/^{204}Pb$ versus $^{207}Pb/^{204}Pb$ plot; however, the $^{207}Pb/^{204}Pb$ values of the RTJ MORB are higher than those of the DM and LCC. In contrast, the CR MORB show large variability in the Pb isotopic composition, consistent with both mixing lines, which may suggest a more heterogeneous mantle contaminated by both the UCC and LCC components (Fig. 5c, d). The UCC contamination signatures are supported by the CR MORB data obtained in this study with the highest radiogenic Pb and lowest $^{143}Nd/^{144}Nd$ compared with the published CR MORB data (Fig. 5). Whereas the 9–10°N MORB which plot closest to the LCC have the least radiogenic Pb compared with the northern Indian Ocean Ridge MORB (Fig. 5c, d). Even though the extremely high $^{87}Sr/^{86}Sr$ and low $^{143}Nd/^{144}Nd$, which characterize the LCC and UCC, are not observed in the CR MORB, the compositional trend defined by the majority of the northern Indian Ocean Ridge MORB do show that the CR MORB (and some RTJ MORB) which deviate from the trend have higher

$^{87}Sr/^{86}Sr$ and lower $^{143}Nd/^{144}Nd$ values than the compositional trend (Fig. 5e, f). The influence of the hotspot material can also increase the radiogenic Pb and Sr; however, the UCC is the most plausible contaminant because the CR 3–4°N MORB with highest radiogenic Pb and Sr in CR MORB are far from the Reunion and Afar hotspots (>2000 km) and the CR 9–10°N MORB which are closer to the Afar hotspots have lowest radiogenic Pb and Sr compared with other northern Indian Ocean Ridge MORB (Fig. 5). Precambrian continental peridotite xenoliths often have unradiogenic Pb similar to that found in LCC (Cohen and O'Nions 1982; Sgualdo et al. 2015); hence, the possibility that the sub-ridge mantle may be contaminated by the continental lithospheric mantle cannot be excluded. However, no matter what the specific contaminant is, the evidence of contamination by the UCC, LCC, and/or continental lithospheric mantle suggests that the CR MORB mantle contains continental lithospheric material.

Basalts from different ridge segments of CR have distinct isotopic compositions with the lowest Pb isotope ratios found in CR 9–10°N and the highest ones in CR 3–4°N (Fig. 5); this is consistent with mantle contamination by continental lithospheric material. In contrast, the contamination signatures in basalts from other CR ridge segments are not significant (Fig. 5). This indicates that the MORB mantle beneath the CR is extremely heterogeneous. The heterogeneity of the CR mantle is strongly expressed by the presence of basalts having $^{206}Pb/^{204}Pb$ lower than 17.5 (Fig. 5). These basalts combined with the low Pb isotope ratios MORB from the RTJ (Price et al. 1986) (Fig. 5) and the SWIR 39–41°E (Mahoney et al. 1992; Meyzen et al. 2005) represent the least radiogenic Pb end member of all Indian Ocean MORB; their low $^{206}Pb/^{204}Pb$ values rule out a plume origin. Old subducted marine sediments also fail to explain the low $^{206}Pb/^{204}Pb$, while an origin from LCC was proposed for extremely low radiogenic Pb of MORB from the SWIR 39–41°E (Meyzen et al. 2005). Ancient continental lithospheric mantle was also proposed as a source of MORB from the SWIR 39–41°E in several studies (Mahoney et al. 1992; Janney et al. 2005). Hence, we suggest that the low Pb isotope ratios in the CR MORB are the result of the melting of mantle contaminated by continental lithospheric materials. Involvement of continental materials in the oceanic mantle can be induced by either destabilization of the ancient continental lithospheric mantle by Mesozoic plume activity (Mahoney et al. 1992) or delamination of the continental lithosphere related to the breakup of Gondwana (Escrig et al. 2004; Ray et al. 2013). These two mechanisms can work effectively in the Indian Ocean ridge because the Indian continental lithosphere is unusually thin (down to ~50 km) (Negi et al. 1986). Evidence indicating the presence of continental lithosphere material in the mantle beneath different ridges in the Indian Ocean suggests that interaction between continental and oceanic lithospheres was prevalent during the opening of the Indian Ocean. Given that the continental lithospheric material was introduced into the asthenosphere before or during the breakup of Gondwana (Mahoney et al. 1992; Janney et al. 2005; Escrig et al. 2004; Ray et al. 2013), it could have been preserved in the asthenospheric mantle for a long time rather than being erased by mantle convection. Thus, the long-term preserved continental lithosphere may play a significant role in producing the isotopic anomaly of the Indian Ocean MORB.

Conclusions

Major and trace element analysis suggest that variations in the composition of MORB from the Carlsberg Ridge are dominated by partial melting variations other than fractional crystallization. Melting of a DM-like mantle with the addition of some enriched components may be responsible for the enrichment of incompatible elements such as K and Rb. The Sr–Nd–Pb isotopic compositions of CR basalts show that the CR mantle is contaminated by both upper and lower continental crust (or continental mantle) components, leading to a heterogeneous mantle on a regional scale (within ~2000 km). These results confirm that significant interactions occurred between the continental lithosphere and oceanic mantle during the opening of the Indian Ocean, suggesting that continental material played a significant role in producing the isotopic anomaly observed in the Indian Ocean MORB.

Acknowledgements We are thankful to the crew and scientists of RV Dayang Yihao Cruise 26. The paper was greatly improved by insightful reviews by two anonymous reviewers. This work was supported by the the MOST of China (2016YFC0600402); the National Basic Research Programme of China (973 programme) (2015CB755905, 2012CB417305); the National Program on Global Change and Air–Sea Interaction, SOA (GASI-GEOGE-01); the Scientific Research Fund of the Second Institute of Oceanography, SOA (JG1603, JG1403); and the National Natural Science Foundation of China (41506073, 41506070).

References

Armienti P, Gasperini D (2007) Do we really need mantle components to define mantle composition? J Petrol 48(4):693–709

Banerjee R, Iyer SD (1991) Petrography and chemistry of basalts from the Carlsberg Ridge. J Geol Soc India 38:369–386

Cann JR (1969) Spilites from the Carlsberg Ridge, Indian Ocean. J Petrol 10(1):1–19

Cannat M, Sauter D, Bezos A, Meyzen C, Humler E, Le Rigoleur M (2008) Spreading rate, spreading obliquity, and melt supply at the ultraslow spreading Southwest Indian Ridge. Geochem Geophys Geosyst 9(4). doi:10.1029/2007GC001676

Chaubey AK, Bhattacharya GC, Murty GPS, Desa M (1993) Spreading history of the Arabian Sea: some new constraints. Mar Geol 112:343–352. doi:10.1016/0025-3227(93)90178-X

Cohen RS, O'Nions RK (1982) The lead, neodymium and strontium isotopic structure of ocean ridge basalts. J Petrol 23(3):299–324

Condie KC (2003) Incompatible element ratios in oceanic basalts and komatiites: tracking deep mantle sources and continental growth rates with time. Geochem Geophys Geosyst 4(1):1–28

Dunn RA, Forsyth DW (2007) Crust and lithospheric structure—seismic structure of mid-ocean ridges. Treatise Geophys 1(12):419–443

Dupré B, Allègre CJ (1983) Pb–Sr isotope variation in Indian Ocean basalts and mixing phenomena. Nature 303:142–146. doi:10.1038/303142a0

Dyment J, Hémond C, Guillou H, Maia M, Briais A, Gente P (2001) Central Indian Ridge and Réunion hot spot in Rodrigues area: another type of ridge–hot spot interaction? Eos Transactions AGU 82:47. Fall Meeting Supplementary T31D-05

Elthon D (1992) Chemical trends in abyssal peridotites: refertilization of depleted suboceanic mantle. J Geophys Res Solid Earth (1978–2012) 97(B6):9015–9025

Escrig S, Capmas F, Dupré B, Allegre CJ (2004) Osmium isotopic constraints on the nature of the DUPAL anomaly from Indian mid-ocean-ridge basalts. Nature 431(7004):59–63. doi:10.1038/nature02904

Füri E, Hilton DR, Murton BJ, Hémond C, Dyment J, Day JMD (2011) Helium isotope variations between Réunion Island and the Central Indian Ridge (17°–21°S): new evidence for ridge–hot spot interaction. J Geophys Res 116:1–17

Gale A, Dalton CA, Langmuir CH, Su Y, Schilling JG (2013) The mean composition of ocean ridge basalts. Geochem Geophys Geosyst 14(3):489–518. doi:10.1029/2012GC004334

Hart SR (1984) A large-scale isotope anomaly in the Southern Hemisphere mantle. Nature 309:753–757

Hekinian R (1968) Rocks from the mid-oceanic ridge in the Indian Ocean. Deep Sea Res Oceanogr Abstr 15(2):195–198

Hemming SR, McLennan SM (2001) Pb isotope compositions of modern deep sea turbidites. Earth Planet Sci Lett 184(2):489–503

Hofmann AW (2003) Sampling mantle heterogeneity through oceanic basalts: isotopes and trace elements. Treatise Geochem 2:61–101

Humler E, Whitechurch H (1988) Petrology of basalts from the Central Indian Ridge (lat. 25°23′S, long. 70°04′E): estimates of frequencies and fractional volumes of magma injections in a two-layered reservoir. Earth Planet Sci Lett 88:169–181. doi:10.1016/0012-821X(88)90055-6

Ito E, White WM, Göpel C (1987) The O, Sr, Nd and Pb isotope geochemistry of MORB. Chem Geol 62:157–176. doi:10.1016/0009-2541(87)90083-0

Janney PE, Le Roex AP, Carlson RW (2005) Hafnium isotope and trace element constraints on the nature of mantle heterogeneity beneath the central Southwest Indian Ridge (13 E to 47 E). J Petrol 46(12):2427–2464

Jenner FE, O'Neill HSC (2012) Analysis of 60 elements in 616 ocean floor basaltic glasses. Geochem Geophys Geosyst 13(2). doi:10.1029/2011GC004009

Klein EM, Langmuir CH (1987) Global correlations of ocean ridge basalt chemistry with axial depth and crustal thickness. J Geophys Res Solid Earth (1978–2012) 92(B8):8089–8115

Liu CZ, Snow JE, Hellebrand E, Brügmann G, von der Handt A, Büchl A, Hofmann AW (2008) Ancient, highly heterogeneous mantle beneath Gakkel ridge, Arctic Ocean. Nature 452(7185):311–316

Mahoney JJ, Natland JH, White WM, Poreda R, Bloomer SH, Fisher RL, Baxter AN (1989) Isotopic and geochemical provinces of the western Indian Ocean spreading centers. J Geophys Res Solid Earth (1978–2012) 94(B4):4033–4052

Mahoney J, Le Roex AP, Peng Z, Fisher RL, Natland JH (1992) Southwestern limits of Indian Ocean Ridge mantle and the origin of low $^{206}Pb/^{204}Pb$ mid-ocean ridge basalt: isotope systematics of the central Southwest Indian Ridge (17°–50°E). J Geophys Res Solid Earth (1978–2012) 97(B13):19771–19790

Mahoney JJ, Frei R, Tejada MLG, Mo XX, Leat PT, Nägler TF (1998) Tracing the Indian Ocean mantle domain through time: isotopic results from old West Indian, East Tethyan, and South Pacific seafloor. J Petrol 39(7):1285–1306

Melson WG, O'Hearn T, Jarosewich E (2002) A data brief on the Smithsonian abyssal volcanic glass data file. Geochem Geophys Geosyst 3(4):1–11

Meyzen CM, Ludden JN, Humler E, Luais B, Toplis MJ, Mével C, Storey M (2005) New insights into the origin and distribution of the DUPAL isotope anomaly in the Indian Ocean mantle from MORB of the Southwest Indian Ridge. Geochem Geophys Geosyst 6(11). doi:10.1029/2005GC000979

Meyzen CM, Blichert-Toft J, Ludden JN, Humler E, Mevel C, Albarede F (2007) Isotopic portrayal of the Earth's upper mantle flow field. Nature 447:1069–1074

Michard A, Montigny R, Schlich R (1986) Geochemistry of the mantle beneath the Rodriguez Triple Junction and the South-East Indian Ridge. Earth Planet Sci Lett 78(1):104–114

Munschy M, Schlich R (1989) The Rodriguez Triple Junction (Indian Ocean): structure and evolution for the past one million years. Mar Geophys Res 11:1–14. doi:10.1007/BF00286244

Murton BJ, Tindle AG, Milton JA, Sauter D (2005) Heterogeneity in southern Central Indian Ridge MORB: implications for ridge–hot spot interaction. Geochem Geophys Geosyst 6(3). doi:10.1029/2004GC000798

Natland JH (1991) Indian Ocean crust. In: Floyd PA (ed) Oceanic basalts. Blackie and Sons, Glasgow, pp 289–310

Nauret F, Abouchami W, Galer SJG, Hofmann AW, Hémond C, Chauvel C, Dyment J (2006) Correlated trace element-Pb isotope enrichments in Indian MORB along 18–20S, Central Indian Ridge. Earth Planet Sci Lett 245(1):137–152

Negi JG, Pandey OP, Agrawal PK (1986) Super-mobility of hot Indian lithosphere. Tectonophys 131(1–2):147–156

Othman DB, White WM, Patchett J (1989) The geochemistry of marine sediments, island arc magma genesis, and crust-mantle recycling. Earth Planet Sci Lett 94(1):1–21

Patriat P, Sauter D, Munschy M, Parson LM (1997) A survey of the Southwest Indian Ridge axis between Atlantis II fracture zone and the Indian triple junction: regional setting and large scale segmentation. Mar Geophys Res 19:457–480. doi:10.1023/A:1004312623534

Price RC, Kennedy AK, Riggs-Sneeringer M, Frey FA (1986) Geochemistry of basalts from the Indian Ocean triple junction: implications for the generation and evolution of Indian Ocean ridge basalts. Earth Planet Sci Lett 78(4):379–396

Raju KK, Chaubey AK, Amarnath D, Mudholkar A (2008) Morphotectonics of the Carlsberg Ridge between 62 20′ and 66 20′ E, northwest Indian Ocean. Mar Geol 252(3):120–128. doi:10.1016/j.margeo.2008.03.016

Ramana MV, Ramprasad T, Kamesh Raju KA, Desa M (1993) Geophysical studies over a segment of the Carlsberg Ridge, Indian Ocean. Mar Geol 115:21–28

Ray D, Misra S, Banerjee R (2013) Geochemical variability of MORB along slow to intermediate spreading Carlsberg-Central Indian Ridge, Indian Ocean. J Asian Earth Sci 70–71:125–141. doi:10.1016/j.jseaes.2013.03.008

Ray D, Misra S, Widdowson M, Langmuir CH (2014) A common parentage for Deccan continental flood basalt and Central Indian

Ocean Ridge basalt? A geochemical and isotopic approach. J Asian Earth Sci 84:188–200

Rehkämper M, Hofmann AW (1997) Recycled ocean crust and sediment in Indian Ocean MORB. Earth Planet Sci Lett 147(1):93–106

Rooney TO, Hanan BB, Graham DW, Furman T, Blichert-Toft J, Schilling JG (2012) Upper mantle pollution during Afar plume–continental rift interaction. J Petrol 53:365–389

Sang BY, Chang WO, Sang JP, Jonguk K, Jai WM (2014) Geochemistry and petrogenesis of mafic-ultramafic rocks from the Central Indian Ridge, latitude 8°–17° S: denudation of mantle harzburgites and gabbroic rocks and compositional variation of basalts. Int Geol Rev 56:1691–1719. doi:10.1080/00206814.2014.955539

Schilling JG, Kingsley RH, Hanan BB, McCully BL (1992) NdSrPb isotopic variations along the Gulf of Aden: evidence for Afar mantle plume–continental lithosphere interaction. J Geophys Res Solid Earth 97(B7):10927–10966

Sgualdo P, Aviado K, Beccaluva L, Bianchini G, Blichert-Toft J, Bryce JG, David WG, Claudio N, Siena F (2015) Lithospheric mantle evolution in the Afro-Arabian domain: insights from Bir Ali mantle xenoliths (Yemen). Tectonophysics 650:3–17

Standish JJ, Dick HJ, Michael PJ, Melson WG, O'Hearn T (2008) MORB generation beneath the ultraslow spreading Southwest Indian Ridge (9–25 E): major element chemistry and the importance of process versus source. Geochem Geophys Geosyst 9(5). doi:10.1029/2008GC001959

Subbarao KV, Kempe DRC, Reddy VV, Reddy GR, Hekinian R (1979) Review of the geochemistry of Indian and other oceanic rocks. In: Ahrens LH (ed) Origin and distribution of the elements. Pergamon Press, Oxford, pp 367–399

Sun SS, McDonough WF (1989) Chemical and isotopic systematics of oceanic basalts: implications for mantle composition and processes. Geol Soc Lond Spec Publ 42(1):313–345

White WM (1991) Trace elements in igneous processes. In: Dasch EJ (ed) Encyclopedia of earth sciences, vol 1. Macmillan, New York, pp 256–307

Winter JD (2001) A introduction to igneous and metamorphic petrology. Printice Hall, New Jersey, p 697